JOURNAL OF CATALYSIS 126, 339–360 (1990)

The Nature of the Iron Oxide-Based Catalyst for Dehydrogenation of Ethylbenzene to Styrene

1. Solid-State Chemistry and Bulk Characterization

M. MUHLER, J.SCHÜTZE, M. WESEMANN, T. RAYMENT,* A. DENT,† R. SCHLÖGL, AND G. ERTL

*Fritz Haber Institut der Max Planck Gesellschaft, Faradayweg 4, D-1000 Berlin 33, Germany; and *Department of Physical Chemistry, University of Cambridge, Cambridge, England; and †Daresbury Laboratory*

Received January 11, 1990; revised June 8, 1990

The active catalyst for the dehydrogenation of ethylbenzene is generated from a precursor material consisting of hematite and potassium hydroxide (with additional promotors) during the initial phase of catalyst operation at 873 K in a steam atmosphere. The active phase is a thin layer of $KFeO_2$ supported on a solid solution of $K_2Fe_{22}O_{34}$ in Fe_3O_4. The ternary $K_2Fe_{22}O_{34}$ phase acts as storage medium from which the active surface is continuously supplied with a near-monolayer coverage of potassium ions in an environment of Fe^{3+} ions. The catalyst undergoes a continuous solid-state transformation caused by the migration of potassium ions. This requires a certain degree of imperfection in the matrix lattice which originates from the catalyst preparation and from the addition of promotors which act on the iron oxide lattice rather than on the surface chemistry. The identity of the active phase with $KFeO_2$ was confirmed by independent synthesis of this phase and comparison of its catalytic activity with that of the technical catalyst.

1. INTRODUCTION

The industrial dehydrogenation of ethylbenzene (etbz) to styrene (sty) has been carried out over promoted iron oxide since 1957 (*1*). In a comparative study of promoted transition metal oxide catalysts it was found that, among the many active systems, an iron oxide-based catalyst promoted by potassium was particularly efficient with respect to both selectivity and activity (*2*). The addition of potassium increased the conversion by one order of magnitude. In the later stages of development, structural promotors like alumina and chromium oxide were added as were promotors for the selectivity such as oxides of V, Ce, W, and Li (*3*), which, however, further improved the catalytic performance only moderately. Any catalyst model may therefore essentially be restricted to systems consisting of iron and potassium oxides.

The reaction of etbz to sty is endothermic (ΔH = 124.9 kJ/mole). The increase in the number of molecules favors the equilibrium toward the product side upon dilution with inert water vapor. In the isothermal process studied here a molar ratio of 6 : 1 water to etbz is used at a temperature of 873 K. Typically, a loading of the catalyst of 0.5 h^{-1} and a resulting contact time of ca. 0.6 s are chosen such that at 50% conversion (equilibrium value 70%) the selectivity with respect to liquid organic by-products is optimized. Typical by-products are 1% benzene and 2% toluene besides traces of methane and ethylene and a few percent CO_2.

Kinetic aspects of this process were studied by several authors. Carra and Forni (*4*) described the reaction by a Langmuir–Hinshelwood mechanism. They found the reaction to be unimolecular and to depend on the adsorption–desorption equilibrium of etbz and sty. The preferred adsorption of sty leads to a site-blocking effect by the product. Further studies by Lebedev *et al.* (*5*)

0021-9517/90 $3.00

and Hirano (*6*) agreed with these findings. They established that water vapor does not participate in the reaction itself but acts purely as inert dilution agent and may be replaced by inert gases. Under practical conditions, however, water is an important ingredient since it continuously regenerates the active catalyst surface and it prevents the total reduction of the iron oxide to iron metal by the hydrogen produced. CO_2 was found to be a reversible poison to the catalyst. The nature of the reaction centers is a matter of controversy: Carra and Forni (*4*) assume one type of active site which generates in parallel reactions all products, whereas Hirano (*6*) postulates a variety of specialized reaction sites. Lee (*2*) describes a study using a differential microreactor with the following essential results: At low conversion the selectivity approaches 100%. When the conversion approaches equilibrium, the selectivity is significantly reduced because of the reduction in the rate of formation for styrene alone caused by product inhibition which does not operate on the rates of formation for the by-products.

Catalyst deactivation (*7, 8*) occurs in two principal ways. Reversible short-term deactivation is caused by extensive CO_2 formation or by deposition of carbonaceous material from product condensation. Treatment with pure water vapor under the influence of the multifunctional promotor potassium as gasification catalyst is used to restore the initial activity. The second mechanism leads to a slow, continuous long-term deactivation. It is caused by a redistribution of the potassium in the catalyst in a twofold manner. Potassium is transported along the reactor with the mass stream and partly removed from the active bed. It is, in addition, removed from the surface of each individual catalyst pellet which is transformed in a solid-state reaction from a homogeneous solid into a potassium-free shell and a potassium-rich core both of which are catalytically inactive.

Several models for the active state of the catalyst have been proposed in the literature. All of them are based upon *ex situ* powder X-ray diffraction data. These data reveal the dominant presence of a spinel phase which is attributed to the isostructural oxide Fe_3O_4 (magnetite) or γ-Fe_2O_3 (cubic hematite). All models have to take into account that potassium ions cannot be incorporated into the close-packed lattice of magnetite because their ionic radius, which is 133 pm, is as large as the oxygen anion radius of 140 pm. This was also confirmed in an experimental study of the solid-state reactivity of the potassium–magnetite system (*9*). All models point to the importance of Fe^{3+} ions for the dehydrogenation process. These somewhat conflicting conditions had to be incorporated into all models proposed.

The model of Lee and Vijh (*2, 10*) suggests no crystal structural but an active surface of iron oxide in which alkali ions are embedded. The promotor action is attributed to local electronic effects. No evidence was found for a direct charge transfer from the alkali to the oxide. A good correlation between the enhancement of activity and selectivity upon promotor addition and the difference in electronegativity between the lattice (Pauling electronegativity of Fe) and the promotor atom was interpreted as a polarization of the iron-to-oxygen bond. The resulting increased electron and proton affinity of the active center should help to activate the substrate etbz.

In the second model (*8*) the catalyst is considered to be a two-phase system consisting of a solid iron oxide support and a liquid potassium hydroxide film. In a technical catalyst the potassium loading would generate a ca. 10,000-pm-thick film of KOH which would be indeed liquid at the operation temperature of 873 K. The presence of CO_2 converts KOH into potassium carbonate, which is solid at the reaction temperature and thus deactivates the catalyst. The model also explains the observed gradients

of the potassium distribution with parallel gradients of CO_2 formation in the catalyst bed. Activation and deactivation relate in this model to the equilibrium between KOH and K_2CO_3. The reaction is thought to proceed at the interface solid/liquid to explain the strong influence of the support oxide on catalytic peformance. Since the diffusion of, in particular, the sty through a thick KOH layer would cause severe losses of product due to polymerization, the model was modified such that the potassium film is not continuous but consists of droplets held in the pore system of the catalyst. This picture allows for a freely accessible solid/liquid interface at the boundaries of the droplets which constitute the active zones of the catalyst (*11*). A severe problem with this model is the fact that the KOH film would evaporate within seconds due to its vapor pressure at reaction temperature which is in contradiction to the stability of the catalyst over several years on stream.

The third model (*12*) suggest $KFeO_2$ as the active phase. This ternary oxide was identified after steam treatment of the catalyst in *ex situ* X-ray diffraction (XRD) data. If the activated catalyst was treated with the poison CO_2 the XRD line for $KFeO_2$ was not observed. In this way a correlation was established between a crystallographic phase (which is difficult to identify due to its peculiar diffraction pattern, see below) and the kinetic performance of the catalyst. The importance of a cycle of solid-state reactions for generation and loss of the active phase was pointed out. This reaction cycle which uses X-ray amorphous Fe_2O_3 and K_2CO_3 as materials can be verified by direct synthesis of $KFeO_2$ from these ingredients but only at 1273 K as compared to the catalyst operation temperature of 873 K.

The last model suggests potassium-doped γ-Fe_2O_3 as the active ingredient. Koppe *et al.* (*13*) performed precision measurements of the lattice parameter of activated catalysts again as a function of steam treatment. In active catalysts the lattice parameter was found to be contracted relative to the value of pure magnetite of 839.4 pm. Pure γ-Fe_2O_3 exhibits a parameter of 835 pm and for the activated catalysts a value of 838.9 pm was determined which was interpreted as being indicative of a defective γ-Fe_2O_3 structure. The defects are assumed to be potassium ions in octahedral lattice sites of the structure which in that way can accommodate 2.3 at.% of the 6.9 at.% potassium present. The authors suggest that the widening of the lattice parameter caused by incorporation of potassium is responsible for increased selectivity of the catalyst because of a better match of the distances of iron centers with the C–C bond length of the substrate etbz. They also suggest a reaction mechanism in which the γ-Fe_2O_3 is reduced to Fe_3O_4 during the dehydrogenation and reoxidized to γ-Fe_2O_3 by steam.

All models point toward the importance of a K–O–Fe^{3+} entity as the active center of the catalyst. All models pose some problems with respect to the description of the formation of these centers under reaction conditions. They either require unusual solid-state chemistry or they cannot explain the stability of the potassium phase. They all consider the catalyst to be in the same state at room temperature in air as under reaction conditions.

The purposes of the present work were to gain an understanding of the nature of the active phase in this catalyst and to describe its formation and deactivation under reaction conditions. A multimethod approach was used, in which X-ray diffraction (XRD) was applied, both *ex situ* and under reaction conditions, to follow the bulk structural aspects of the catalyst. These results together with those from auxiliary techniques, such as surface area determination, thermogravimetry, EXAFS, and Mössbauer spectroscopy, are described in this paper, Part 1. The characterization of the surface of the catalyst used under technical reaction conditions in a microreactor coupled to a surface analysis instrument by XPS and UPS

TABLE 1

Bulk Elemental Composition (mol%) of the Precursors

	Fe	K	Al	Cr	V	W	Li	Ca	O
Cat 1	32.8	5.5	0.7						60.9
Cat 2	32.7	5.5	0.7		0.4				60.7
Cat 3	31.8	5.6	0.7		0.3	0.3	2.7		58.5
Cat 4	30.1	5.5		0.8				2.1	61.4

will be described in Part 3 of the series. An interconnection between bulk and surface analysis will be made by a characterization of the active catalyst morphology at all levels of organization (Part 2).

2. EXPERIMENTAL

A variety of catalyst precursors were obtained from BASF, Ludwigshafen. The bulk elemental composition of the samples used in this work is described in Table 1. All catalysts contained iron and potassium in a fixed, atomic ratio of ca. 6:1; the typical iron to oxygen ratio is 1:2. The catalysts were used either as 6-mm-diam pellets or, for the microreactor studies, as 1-mm sieve fractions of crushed pellets. Long-term deactivation was also studied with technical samples of catalyst 4 used for 300 days on stream and with samples used for production for over 2 years. All samples are air sensitive due to their high content of alkaline material and were kept under an inert gas atmosphere. The model compounds $KFeO_2$ and $K_2Fe_{22}O_{34}$ were synthesized according to Ref. (*14*) in a platinum crucible at 1223 K in air.

Nitrogen BET isotherms were determined with the flow method using a Quantachrome Jr II instrument. Thermogravimetry was performed with a modified Perkin-Elmer TGS 2 instrument in various gas atmospheres. Heating rates between 3 and 10 K/min were used: with a minimum sample weight of 4 mg, 10 K/min was found to be sufficiently slow. Analysis of the weight losses was performed on a Mettler TGA 7 instrument coupled to a Balzers QMG 501 mass spectrometer.

XRD was performed *ex situ* on a focusing Guinier diffractometer (Huber) using monochromatized CoKα radiation. Samples were rapidly quenched after catalytic testing and transferred into a silicon grease giving no background in the 2θ range of interest. This preparation method for transmission diffraction analysis, which required ca. 10 min after stop of the feedstock, resulted in samples which only slowly decomposed under the influence of air as was revealed by several runs on the same sample recorded consecutively. All data were recorded using silicon as internal standard. The *in situ* experiments were done on a modified Philips APD 10 instrument equipped with a modified Anton Parr HTK 10 camera which allowed heating of the sample mounted on a platinum support to 873 K in an atmosphere of ca. 10:1 water vapor to ethylbenzene. The styrene formed polymerized to a large extent on the cold parts of the camera. The platinum reflections were used as internal standard for the 2θ scale.

EXAFS experiments on the Fe and Cr K-edges were measured on station 7.1 at Daresbury Synchotron Radiation Source. The Fe spectra were measured in transmission mode at 77 K using powdered samples diluted with boron nitride to give an absorption edge jump of 1–2. The Cr spectra were recorded in transmission mode and as fluorescence spectra using scintillation detectors since the samples were only 0.7 at.% chromium. Transmission data were collected on the reference materials hematite, magnetite, and iron powder and on analytical-grade samples of Cr^{3+} and Cr^{6+} oxides. The SRS was operating at an energy of 2.0 GeV with an average current of 150 mA. An order sorting Si(111) monochromator was used to minimize the harmonic contamination in the monochromatic beam. Pre-edge and post-edge background subtraction was performed using the Daresbury EXBACK program which employs a polynomial form for the smoothly varying atomic absorption

TABLE 2

Precision Lattice Constant Measurements. 0^a (pm)

Cat 4	839.9
Cat 4, 2 h H_2O	839.1
Cat 3	838.2
Cat 1, oxidized	838.0 + 834.5
Fe_3O_4	839.4
γ-Fe_2O_3	835.0

coefficient. Data analysis utilized rapid curve wave single scattering theory (*1, 2*) in the program EXCURV88 (*3*) on the raw (i.e., unfiltered) α^{-3} weighted EXAFS data. Phase shifts were calculated within EXCURV88 and then empirically modified so that the structural parameters for standard compounds agreed to within experimental error with their accepted values. Further details of model fitting can be found in reference 4. Reference materials and were magnetite, iron powder, and analytical-grade samples of Cr^{3+} and Cr^{6+} oxides.

Mössbauer spectra were recorded in transmission with absorber temperatures between 1.2 and 300 K. The absorbers were prepared under Ar with catalyst powders diluted in BN and encapsulated in airtight containers with Be windows. A ^{57}Co (Rh) source at 300 K was used. Calibration of the isomer shift [$\delta(\alpha\text{-Fe}) = 0.0$ mm/s] was performed with a stainless-steel foil.

3. RESULTS

3.1. Surface Area and Porosity

The four catalysts were characterized by dynamical nitrogen adsorption before and after use in the microreactor. The porosity of the precursors was also measured by the Hg penetration method. BET surface areas were determined from the linear part of the adsorption isotherm leading to the results listed in Table 2. The BET surface areas were independent from the degas temperatures which were chosen to be above (650 K) as well as below (400 K) the melting point of KOH, indicating that there is no migration of liquid KOH into the pore system of the catalyst during the degas period of 17 h. The surface areas are small, as expected after the high calcination temperature of the precursor of ca. 1200 K. The spread in surface area between the catalysts is not correlated to the activity which in all cases reached the industrial value of 50% conversion. Activation of the catalysts led in all cases to a measurable loss of surface area. This loss does not progress with time, since catalysts which have been 2 years on stream exhibit the same surface areas between 2.9 and 2.3 m^2/g. Also, poisoning of an active catalyst with CO_2, which should affect any liquid layer of KOH, does not change the surface area. In an experiment with cat 3 the initial surface area of 3.3 m^2/g dropped after activation and 1 week on stream to 2.6 m^2/g and, after CO_2 poisoning, only to 3.0 m^2/g. The surface area of the catalyst also stays fairly constant over the length of the catalyst bed. A sample of cat 3 used in a 125-cm reactor bed was divided into seven fractions and the surface areas of the material were found to average 2.3 m^2/g, except for the inlet fraction exhibiting 2.9 m^2/g. The core material of a long-term deactivated catalyst is at 0.8 m^2/g much smaller in surface area, reflecting its greater apparent density.

The catalyst material is too brittle to sustain the mechanical stress of Hg porosimetry. This is reflected by the much larger values for surface area resulting from application of this method (see Table 2). A large contribution to this value originates from a large peak in the pore size distribution in the mesopore range. This coexistence of meso- and macropores is also an artifact of the method. The BET data gave no evidence for the existence of meso- or micropores. The absence of such pores in both the precursor and the activated catalyst can be seen from inspection of Fig. 1 which shows modified α-s plots for cat 3. The modification was to use a standard isotherm of ASTM certified pore free calzite determined on the present instrument, scaled to the

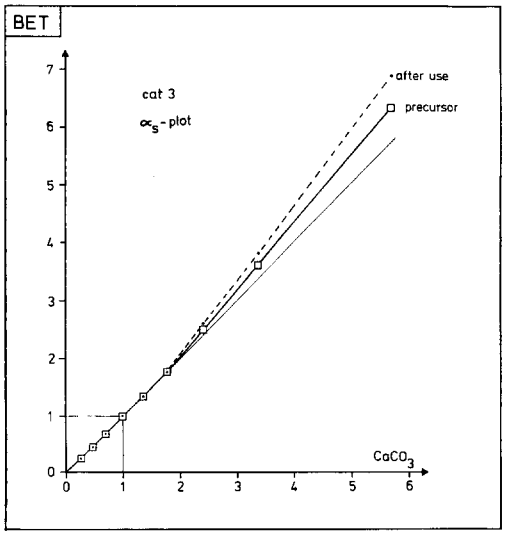

FIG. 1. α_s plot of the nitrogen BET isotherms of cat 3 before and after use. ASTM-certified $CaCO_3$ free of micropores and mesopores was used as reference.

standard isotherm given in Ref. (*15*) in order to account for the effects of the dynamical method on the lineshape of the type II BET isotherm.

In summary, the surface areas of the catalysts are low and decrease even further after activation. No systematic trend of these variations with conversion or time on stream or location in the catalyst bed was found. All catalysts are only macroporous systems which develop a core of very-low-surface-area material during long-term deactivation. No evidence was found for a modification of the surface area by formation of a KOH layer or droplets, nor did fixation of KOH by CO_2 treatment cause any appreciable change in surface area.

3.2. Thermogravimetry

Thermal analysis in various gas atmospheres was used to study the stability of precursors and activated catalysts against reductive thermal decomposition. In this way it was tested whether the promotors influence the reduction of the merely Fe^{3+}-containing precursor materials to magnetite, which is thermodynamically stable under reaction conditions. Reduction in pure hydrogen was used to probe the solid-state reactivity of various catalysts.

The data shown in Fig. 2 reflect the stabilities of various precursor oxides in a mildly reducing atmosphere. All samples lose chemisorbed water between 60° and 150° above room temperature. Samples 1 and 2 exhibit a second weight loss at exactly the reaction temperature of 600°C. This second loss is associated with the evolution of both water and molecular oxygen. At slower heating rates and in ultrapure nitrogen cat 1 loses 25.5% of its weight between 550 and 650°C, which corresponds to a nearly complete loss of all oxygen at the catalyst operation temperature. The weight loss is reversible leading to Fe_2O_3. Addition of promotors such as V (cat 2) or V + W + Li (cat 3) strongly decreases or even suppresses the loss of lattice oxygen and structural water at catalyst operation temperature. We conclude that the promotors lower the chemical reactivity of the precursor oxide matrix consisting of only Fe^{3+} ions.

This is supported by the different reactivity of the catalysts against total reduction in pure hydrogen. The top traces in Fig. 3 demonstrate the stabilizing effect of the promotors by an increase in reduction temperature of 110°C. Cat 2 is quite similar to

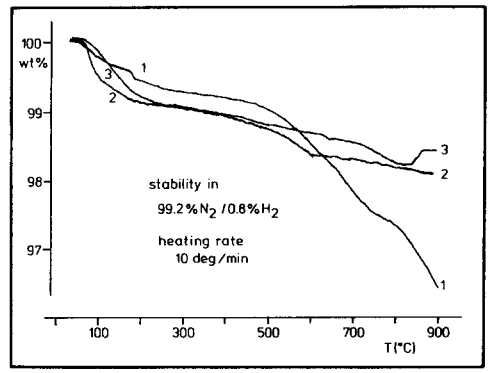

FIG. 2. Weight loss curves of catalysts 1–3, before use in a mildly reducing atmosphere. The flow rate was ca. 10 ml/min. The catalyst operation temperature is at 600°C.

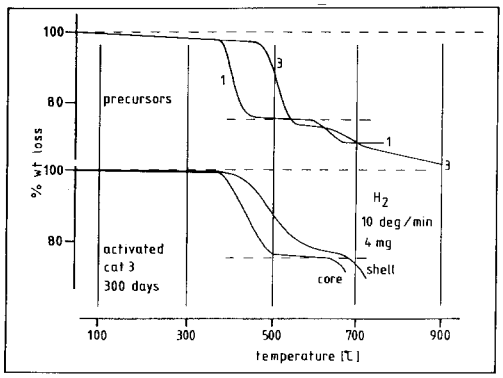

FIG. 3. Reactivity of cat 1 and cat 3 against total reduction in hydrogen. The precursors show different reaction temperature intervals, whereas after catalytic use all catalysts exhibit the same characteristics displayed in the lower part of Fig. 3. The indicated weight losses represent total conversion of iron oxide to iron metal.

cat 3 in behavior, indicating little additional effect of W and Li over V. It is also apparent that neither potassium nor alumina exert a structure-stabilizing effect. The weight losses exceeding the value expected for the conversion of oxide to metal (indicated by the dashed lines in the figure) are spurious effects caused by particles falling off the balance during the release of internal stress of the reduced catalyst particles.

Activated catalysts exhibit broad and poorly reproducible weight loss curves in this experiment. This is due to a coexistence of two materials within the black powder material. Aged catalysts can be mechanically separated into a core and a shell material (see also Part 2). If these two phases are analyzed separately, traces result such as the lower curves of Fig. 3. The shell material is of similar stability as the precursor oxide. The core material exhibits a markedly lower reduction temperature close to that of the unpromoted catalysts. The different shapes of the curves may be correlated with different morphologies as will be outlined in Part 2 of this series.

The core material consists of a significantly more reduced iron oxide than the shell or even the precursor. If these three samples are heated in oxygen, up to 450 K, no weight change except the desorption of water is observed for the vanadia-promoted precursor and the shell material. The core material takes up 4.5 wt% oxygen in the temperature range between 600 to 780 K. This oxygen is released again above 870 K, a temperature at which the unpromoted catalyst loses water in an oxygen atmosphere.

All three catalysts contain the same amount of potassium. Promotion changes the chemical reactivity of the potassium compound. This was verified by heating the samples in a CO_2 atmosphere. KOH should convert at higher temperatures to a carbonate detectable by the associated weight gain. Potassium carbonates should, in turn, release CO_2 upon heating in inert gas (nitrogen) atmosphere. With all samples no characteristic CO_2 evolution was observed up to 1000 K, indicating that the preceding calcination had destroyed all carbonates in the precursor mixture. The promoted catalyst precursors were also inert in the CO_2 atmosphere, indicating the absence of significant amounts of KOH. The unpromoted sample showed, however, an increase in weight by ca. 0.4 wt% at 600 K which would be consistent with conversion of most of the KOH loading to carbonate.

In summary we learn from these experiments that the solid-state reactivity of the precursor oxide at catalyst operation temperature is high and that stabilization of the trivalent iron oxide by addition of promotors like V, W, and Li can be achieved. Used catalysts contain two oxide phases with different chemical reactivity against hydrogen. The material which prevails in the core of aged catalysts can be reoxidized and is not stable against thermal decomposition. The process of segregation associated with the deactivation of the promoted catalysts locally separates the promotor oxides as it concentrates the potassium in the core material. Addition of the promotors also influences the chemical reactivity of the potassium phase in the catalyst precursors. Un-

promoted catalysts contain potassium as hydroxide whereas promoted catalysts contain this element in a chemically inactive form which does not react with CO_2, but is not present as carbonate.

3.3. X-Ray Phase Analysis

Powder X-ray diffraction at room temperature was carried out with the calcined precursor mixtures and with rapidly quenched samples of activated catalysts. Preparation in grease excluded the influence of moisture and CO_2 from the air. This influence was studied in detail by monitoring the changes in relative intensity of the XRD pattern as a function of exposure time to ambient air. It was found that storage of either precursors or, in particular, activated catalysts in air between 1 day and several months resulted in the formation of crystalline phases of potassium carbonate and hydroxocarbonates which all are not genuine components of the catalyst phase mixture.

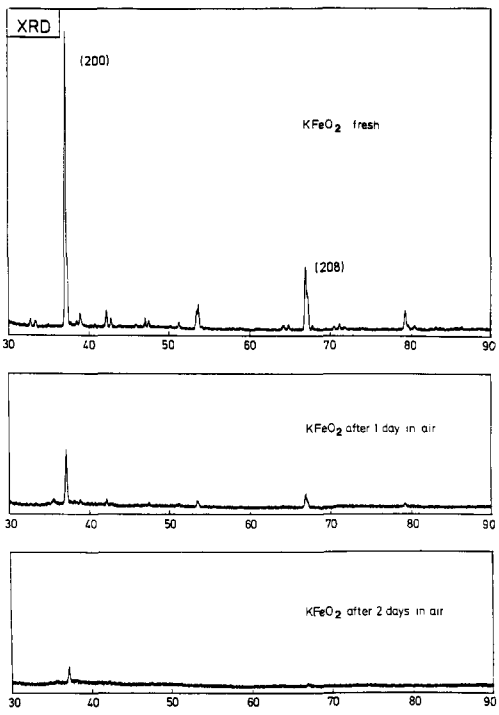

FIG. 4. Guinier transmission powder patterns of $KFeO_2$: top, fresh; center, after 1 day in air; bottom, after 2 days in air. The exposure series was done with the same sample. Radiation: monochromated Co$K\alpha_1$. We note the few reflections of this material in a wide 2θ range.

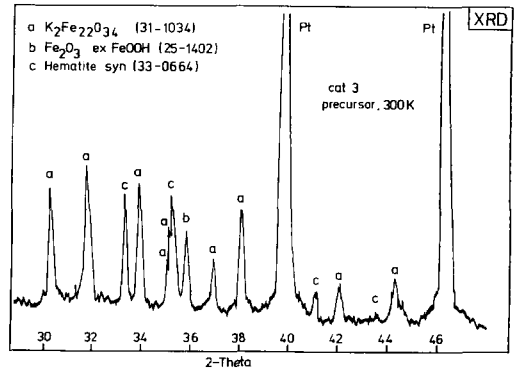

FIG. 5. Part of the powder diffraction pattern of cat 3 before use. The platinum reflections from the sample holder are used as internal reference for the 2θ scale. The numbers in the assignment refer to the JCPDS index. Radiation: postmonochromated Cu$K\alpha$.

A particular example of the air sensitivity of a relevant oxide phase is shown in Fig. 4. The diffraction pattern of a fresh sample of $KFeO_2$ is compared with the data recorded after exposure to ambient air. It turns out that this phase decomposes into entirely X-ray amorphous materials, a process which can be followed visually as a color change from green to red. The structure of this ternary oxide is loosely packed consisting of $Fe^{3+}O_4$ tetrahedra linked via corners, as in the cristobalite structure, with the K^+ ions located in the large cavities with 12-fold coordination formed by the tetrahedral network (*16, 17*). This open structure reacts with moisture leading to hydrated iron oxide and KOH which melts in its own hydration water, transforming the loose oxide powder into a sticky material after ca. 2 days in air.

3.3.1. The precursors. The red catalyst precursors diffract X rays only poorly but do not show any sign of highly disordered crystallinity such as modulated backgrounds or pronounced footing of the Bragg reflections. A fully indexed diffraction pattern of catalyst 3 is shown in Fig. 5. The

pattern consists of three phases two of which are synthetic α-Fe_2O_3; the third phase is a ternary potassium iron oxide, $K_2Fe_{22}O_{34}$. The powder patterns of the two binary iron oxide places, which match well also outside the window, show that the data reported in the JCPDs file are probably for polymorphs of α-Fe_2O_3 with varying contents of water (Fig. 5).

The structure of this oxide is closely related to the spinel structure. It is based upon a cubic close packing of the oxygen anions. The cations are placed in tetrahedral and octahedral gaps. One unit cell contains four FeO_4 tetrahedra and four Fe_4O_4 octahedra which are built into a large face-centered cube of Fe ions. These 8 subunits are stacked such that octahedra are surrounded by tetrahedra and vice versa. If the unit cell is intersected in (200) one obtains two "spinel blocks" consisting of two tetrahedra and two octahedra and $4 \times \frac{1}{4}$ iron ions from the large cube resulting in a sum formula of $Fe_{11}O_{16}$. The ternary oxide is made from two such spinel blocks with a layer of potassium oxide inbetween. The oxygen anions belong to each face of the spinel block, resulting in an overall stoichiometry of $K_2Fe_{22}O_{34}$. The potassium layer is not dense at this stoichiometry, giving rise to a nonstoichiometry between K : Fe 1 : 11 and 1 : 5. The phase is known to be a fast potassium ion conductor (*18, 19*) and to have metallic conductivity due to a small deficiency in the Fe^{3+} content.

This ternary oxide is not present as an X-ray crystalline phase in all catalyst precursors. The diffraction patterns of a large number of precursors were investigated and only the content of synthetic hematite was found to be common to all of them. Some diffraction patterns contain phases of oxides which could not be identified on the basis of the JCPDS data file. There was no apparent correlation between the phase analysis of the precursor and the catalytic behavior of the activated material.

3.3.2. The Activated Catalyst. All activated catalysts exhibit the same diffraction pattern regardless of the large structural differences of the precursor materials if they are investigated as rapidly quenched samples without contact to air. A typical diffraction pattern of catalyst 3 after several days on stream is displayed in Fig. 6. The material consists essentially of highly crystalline magnetite. Only one single reflection at 37.1° 2θ (Co$K\alpha$ radiation) indicates the presence of $KFeO_2$ as a second phase in the active catalyst material. This small peak is the main reflection (200) of the pattern displayed in Fig. 4. Its broad and asymmetric lineshape indicates significant disorder. The small intensity of the $KFeO_2$ line cannot be taken as indicating only a small concentration of this phase at reaction conditions because of its metastable nature at room temperature.

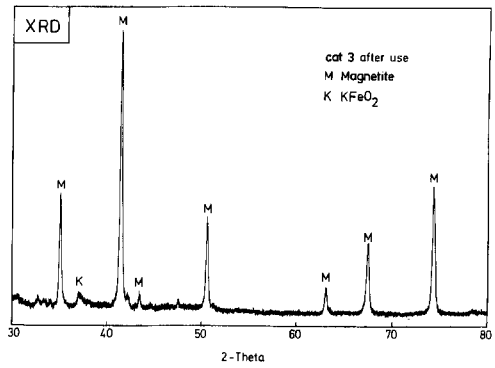

FIG. 6. Guinier transmission diffraction pattern of cat 3 after use. The sample was rapidly quenched and transferred immediately from the microreactor without any exposure to air. The inset shows an enlargement of the profile of the (220) reflection of $KFeO_2$. Its lineshape indicates a strong texture of anisotropic crystals.

Aged catalysts exhibit the effect of disintegration into a core and shell structure. Despite differences in some properties of these materials their XRD traces are similar, and as shown in Fig. 7, both materials consist predominantly of magnetite. The core sample exhibits additional reflections between ca. 25° and 35° 2θ (Cu$K\alpha$ radiation) that may be due to a potassium phase according to wet chemical analysis and EDA analysis of the core samples which is, however, not

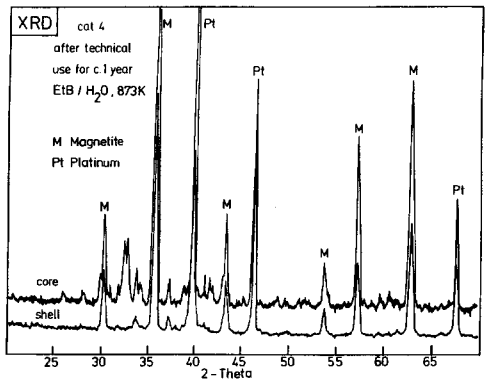

FIG. 7. Comparison of the diffraction patterns of core and shell material isolated from cat 4 after technical use for ca. 1 year. The core material exhibits reflections between 30° and 40° 2θ which cannot be indexed to a known phase in the JCPDS file.

identical to any phase in the JCPDS data base. The pattern excludes the presence of crystalline potassium carbonate which is postulated by the SLP model (*8*).

3.3.3. Precision Lattice Constant Measurements

All activated catalysts exhibit a pronounced pattern of highly crystalline magnetite which crystallizes in the inverse spinel structure. This structure is also adopted by γ-Fe_2O_3 containing only Fe^{3+} ions. As pointed out above and suggested by the model of Koppe *et al.* (*13*), the content of Fe^{3+} is important for the catalytic action of the material. Determination of the oxidation stage of the iron ions in the oxide lattice is thus of importance. According to the Koppe model the oxidation stage of some of the iron ions is expected to oscillate during catalytic action between Fe^{2+} (magnetite) and Fe^{3+} (γ-Fe_2O_3), with steam from the reaction mixture oxidizing the Fe^{2+} ions. Both oxides exhibit the same crystal structure as governed by the packing of the oxygen anions. The different charges on the cations lead, however, via electrostatic forces to a slight contraction of the lattice constant with increasing Fe^{3+} content In addition, the two structures differ with respect to their cation ordering, giving rise to weak superlattice spots which can, however, unfortunately not be measured with polycrystalline powders. The lattice constant varies linearly with Fe^{3+} content between 839.5 pm for Fe_3O_4 and 835.0 pm for γ-Fe_2O_3 according to Vegard's law. Precision measurements of the Bragg peak positions for high-indexed reflections (here 440) allow, with a variation of ca. 0.5° 2θ (Co$K\alpha$ radiation), an accurate determination of the degree of oxidation of the iron in the oxide matrix. The results of such measurements are displayed in Fig. 8 and Table 2 and lead to the following conclusions. The lineshapes of all samples treated under reaction conditions are similar and indicative of a single species. Only oxidation

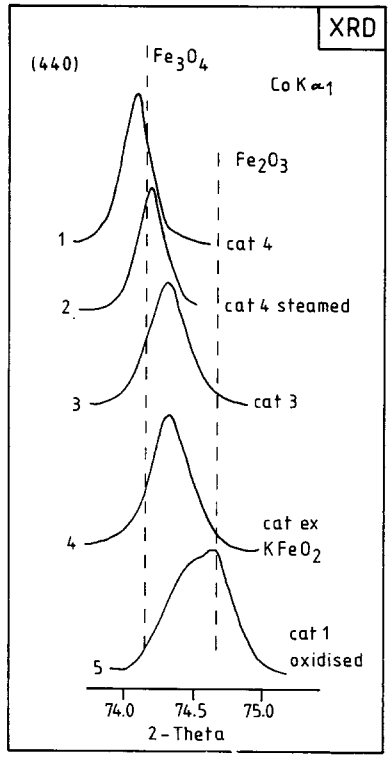

FIG. 8. High-resolution profiles of the (440) reflections of some used catalysis obtained with the Guinier transmission diffractometer. The reference positions were determined from authentic oxide samples with the present instrument and agree well with literature data.

of the activated cat 1 (see profile 5) after evacuation from the reaction mixture and cooling in air led to the broad line consisting of a component of parent catalyst (similar to cat 3) and the expected line at the position of γ-Fe_3O_3. This experiment shows that the method actually works and that the complex lineshapes described by Koppe *et al.* arise from oxidation in (wet) air and not from the action of oxygen-free steam. This treatment which models the reaction conditions causes only a slight shift in the expected direction (see profiles 1 and 2). The unpromoted model catalyst ex $KFeO_2$ exhibits the same lattice parameter as the activated catalysts 3 and 1 which is indicative of a magnetite with some excess Fe^{3+}. Catalyst 4, which was similar in activity to catalyst 3, exhibits a larger lattice parameter indicative of a lower Fe^{3+} content. This unexpected apparent structural difference between the catalysts can be rationalized by taking into account the effect of promotor ions. Assuming that divalent calcium is built into the lattice of cat 4, the amount of 2.1% gives rise to a lattice expansion of ca. 1 pm (*9*) accounting for more than half of the difference in the lattice parameter. The promotor effect of aluminum being present in all catalysts can be neglected with 0.2 pm (*9*).

In summary, the magnetite of all activated catalysts contains Fe^{3+} ions in excess without showing indications for significant disorder (narrow line profiles). Steam treatment under exclusion of air influences the lattice parameter only slightly, whereas oxidation in air leads to a transformation of the nonstoichiometric magnetite into γ-Fe_2O_3. The nonstoichiometric magnetite is also generated by the use of pure $KFeO_2$ as catalyst precursor. The effect of steam treatment described by Koppe *et al.* seems to be of the type of oxidative hydrothermal synthesis as required for the topotactic solid-state reaction equilibrium between Fe_3O_4 and γ-Fe_2O_3:

$$8Fe_t^{3+}\,(8Fe^{3+}8Fe^{2+})_o\,32O^{2-} \rightarrow 8Fe_t^{3+}\,(12\,Fe^{3+}\,4\square)_o\,Fe^{3+}\,O\overline{H}\,31O^{2-}.$$

The subscripts t and o designate the cation coordinations tetrahedral and octahedral. The equilibrium at high temperatures is controlled by the partial pressures of water and oxygen. Steam itself is not an oxidizing agent in the system but is required as a source of structural water essential for the formation of γ-Fe_2O_3 (*20*).

The determination of the degree of oxidation by lattice constant measurements is influenced by the countereffect of promotor cations. As a consequence, only qualitative conclusions can be drawn. Further specific information is required about the oxidation state of the iron in the catalysts which was obtained by Mössbauer spectroscopy (MAS).

3.4. Mössbauer Spectroscopy

This technique had already been applied previously to the present system (*21*). The authors found only magnetite in used catalyst samples. Their samples were, however, of ill-defined prehistory. In the present work samples of catalysts 1 and 3 were activated in the microreactor (see part 3) and then rapidly transferred under strict exclusion of air into vacuum-tight absorber holders with Be windows. The spectra of the two catalysts were similar and also little difference was found in a sample of catalyst 4 after technical use for ca. 300 days on stream. Typical room-temperature spectra are displayed in Fig. 9, and the corresponding hyperfine parameters and reference values are summarized in Table 3. The patterns indicate the presence of magnetite (*22*) which is in agreement with the value for the internal magnetic field for both octahedral and tetrahedral sites. The shape of the pattern clearly excludes the presence of γ-Fe_2O_3 as bulk phase in the active catalyst. The isomer shift and the area ratio between octahedral and tetrahedral sites are, however, significantly different from the parameters of pure magnetite. The difference in the isomer shift of 0.1 mm/s for both sites is an indication of a lattice distortion influencing the average *s* electron density at the iron nucleii. The area

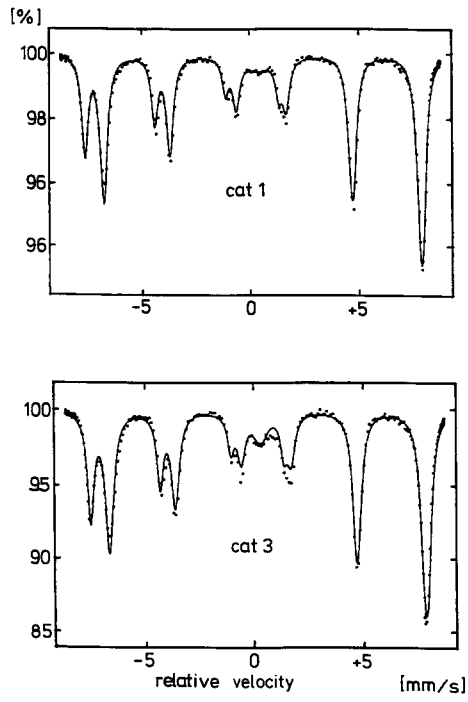

FIG. 9. Mössbauer spectra of cat 1 and cat 3 after use in the microreactor. The fit includes two sites for the spinel oxide and an additional contribution in the central part of the spectra. The acquisition temperature was 300 K; samples were held in airtight containers.

ratio is at 1.66 identical to that of γ-Fe_2O_3 which can be considered as an entirely disordered spinel structure with a random distribution of only Fe^{3+} at tetrahedral and octahedral sites. In magnetite Fe^{2+} ions occupy the octahedral sites. Partial oxidation of these ions would increase the occupation of the tetrahedral sites which is in agreement with the experimental low ratio of the o/t occupation of 1.66. To account for this value all Fe^{2+} ions would have to be oxidized which is in clear contradiction to the parameters of isomer shift and internal hyperfine field. Thus, additional Fe^{3+} ions must occupy the vacancy system of the spinel structure. These ions do, however, not form a crystallographic phase of their own (such as the reference compounds listed in Table 3) which would give rise to additional doublets or even six-line patterns. The deviation of the area ratio for the two sites from that of the reference magnetite data indicates the existence of a solid solution of an additional phase in magnetite.

The central region of the spectra exhibits additional absorption indicative of a broad line. The isomer shift of this magnetically nonsplit line is at 0.30 to 0.40 mm/s indicative of a third crystallographic phase consisting of Fe^{3+} ions. This line, which is only partly accounted for in the model shown in Fig. 9, has been fitted to different patterns including a narrow doublet and a broad single absorption. None of these fits was in satisfactory agreement with either the spectrum or known parameters for chemically reasonable compounds. This is ascribed to the existence of a distribution of spectral parameters the resolution of which is below the possibilities of such a low-intensity component. This phase can be assigned to $KFeO_2$ with the variation in isomer shift being indicative of a varying structural disorder. The $KFeO_2$ crystals are of very small size which leads to a collapse of the expected six-line pattern into a single line (superparamagnetism). The effect was checked by accumulating spectra also at 78 and 4.2 K without a change in the central region of the spectrum. A more detailed analysis of the low-temperature spectra is difficult due to the increased complexity of the pattern introduced by the Vewey transition of magnetite at 120 K (*23*).

The MAS data suggest, in summary, that the active catalyst consists of a spinel matrix and a small amount of structurally ill-defined $KFeO_2$. The spinel structure is neither pure magetite nor γ-Fe_2O_3 but may be described as a solid solution of a Fe^{3+} compound within the magnetite lattice. This distorted lattice may be described as a sequence of spinel blocks with some of them containing stacks of $(KO)^-$ layers. The additional negative charges from the potassium oxoanions are compensated by the partial oxidation of Fe^{2+} ions. In this way the material is a continuous intergrowth of magnetite with $K_2Fe_{22}O_{34}$, a view which is consistent with

TABLE 3

Hyperfine Parameters, δ (mm/s) and H (kG)

	Cat 1	Cat 3	Fe_3O_4	$KFeO_2$	γ-Fe_2O_3	$K_2Fe_{22}O_{34}$
δ^t	0.16	0.17	0.26	0.44	0.27	0.13–0.27
δ^o	0.55	0.54	0.65		0.41	0.31–0.41
δ^c	0.40	0.29				
H_{eff}^t	483	479	489	512	488	495.487
H_{eff}^t	452	447	458		499	518.438
o/t	1.66	1.67	1.93		1.66	1.75
%t	35.7	35.7				
%o	59.5	59.6				
%c	4.8	4.8				

the XRD results. Such a model solves the problem of storing variable amounts of potassium in the iron oxide lattice of the catalyst matrix. It does not require a second phase of a binary potassium compound as, e.g., a liquid film, without contradicting the commonly accepted view of the catalyst consisting of a spinel iron oxide matrix. EXAFS was used to exclude the presence of any additional iron oxide species which might be present in amorphous form, and to detect the location of the promotor ions.

3.5. EXAFS Analysis

EXAFS data of the Fe K edge were recorded to gain more insight into the nature of the spinel phase and the details of the Fe distribution in the dense oxygen anion packing. The role of the transition metal promotors was studied by analyzing the EXAFS of chromium as an example.

A series of samples of cat 4 which had been on stream between 3 and 600 days and a sample of used cat 3 were analyzed together with the precursor materials and the reference materials Fe_3O_4, α-Fe_3O_3, and $K_2Fe_{22}O_{34}$. The EXAFS spectra of both precursors were very similar to that of α-Fe_2O_3 which was fitted to the known crystallographic structure serving as reference for the phase shift parameters.

The spectra of the used samples of cat 4 were very similar, indicating that after activation the material remains essentially unchanged until it spatially disintegrates into the core and shell phases. Figure 10 shows the EXAFS spectrum of cat 3 after 1 year on stream. The spectrum is of good quality also at high k values. The fit shown is a model describing the first four coordination shells. The resulting radial distribution function is compared with those of reference compounds in Fig. 11. Selected parameters of the corresponding fits and their comparison to the X-ray structures are listed in Table 4. The crystal structure of β-alumina served as model for $K_2Fe_{22}O_{34}$, the structure of which has not been determined by single-

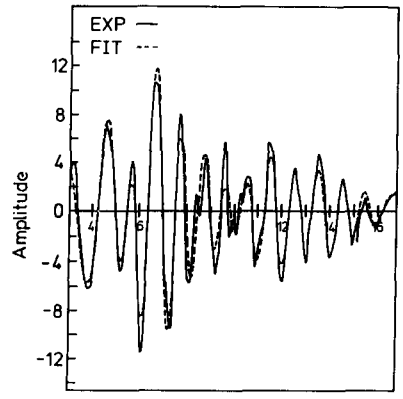

FIG. 10. EXAFS spectrum of a used sample of cat 3. The fit shown is the back Fourier transform of a model for the first four coordination shells.

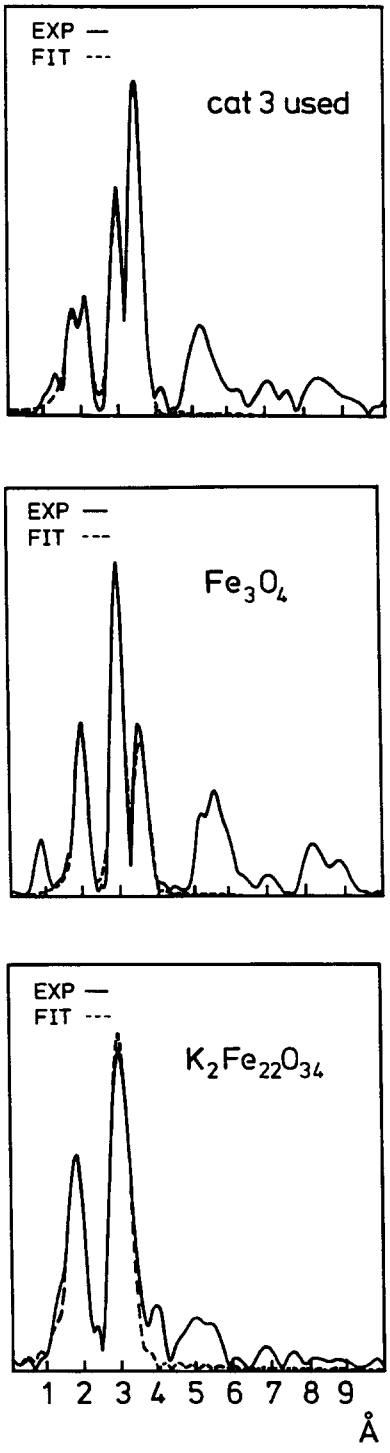

FIG. 11. Experimental and fitted radial distribution functions for used cat 3, and the reference compounds Fe_3O_4 and $K_2Fe_{22}O_{34}$. We note the significant difference in intensity distribution of the higher coordination shells between magnetite and the catalyst.

crystal X-ray methods. From both the figure and the table it can be seen that the maxima in the radial distribution function are rather similar for the three compounds. The intensity distribution is, however, significantly different in the spectra of the catalyst and the magnetite. The spectra of all catalysts consistently show a splitting of the first peak which is due to equal occupation of the first two oxygen coordination shells, whereas the reference compounds exhibit single peaks due to the dominant occupation of one of them. Even more drastic is the difference between magnetite and the catalyst in the occupation of the first two iron shells. This is in full agreement with the Mössbauer results which also demonstrate a deviation of the iron distribution in the catalyst compared to magnetite. The strong overlap in the positions of the maxima in the radial distribution functions prevents the identification of a mixture of $K_2Fe_{22}O_{34}$ in the spinel matrix by fitting procedures. The observed difference in intensity distribution between the catalyst and magnetite may, however, indeed be due to a superposition of the spectra of magnetite and $K_2Fe_{22}O_{34}$ in the catalyst spectrum.

The radial distribution function of cat 3 is quite different from that of cat 4. It deviates even more from that of magnetite. The occupation of the iron shells relative to the unchanged occupation of the oxygen shells is significantly reduced leading to an almost vanishing peak at 3.44(2) Å (occupation 1.0) compared to the most intense peak in the spectrum of cat 4 at 3.46(2) Å (occupation 2.8). The good reproducibility of the data set of cat 4 allows us to conclude that this effect is characteristic of the catalyst types which differ in their promotor content. Addition of vanadium, tungsten, lithium, and alumina in cat 3 instead of chromium and calcium in cat 4 profoundly modifies the distribution of the majority of the iron atoms in the structure. This effect, which is caused by the presence of a small amount of impurity atoms, seems to influence only the local coordination since in XRD both catalysts appear to be magnetite. The precision lattice constant determination, however, gives a

TABLE 4

EXAFS Parameters

Shell	Occupation (±1)	Type	Radius[a] (Å)	Radius from x ray (Å)
		Sample cat 4 used		
1	2.2	O	1.90	
2	1.8	O	2.05	
3	3.0	Fe	2.97	
4	2.8	Fe	3.46	
		Sample Fe_3O_4		
1	1.3	O	1.84	1.82
2	4.0	O	2.00	2.10
3	4.0	Fe	2.97	2.96
4	8.0	Fe	3.49	3.48
		Sample $K_2Fe_{22}O_{34}$		
1	2.5	O	1.94	1.91
2	1.1	O	2.17	2.01
3	2.9	Fe	2.97	2.97

[a] ±0.02.

small indication of the large difference in local coordination with its smaller value of 8.382 Å for cat 3 compared to 8.394 Å for magnetite and cat 4.

Iron EXAFS has shown that the local coordination of iron to oxygen in the catalysts is different from the coordination in magnetite. Comparison of differently promoted catalysts demonstrates that small amounts of additives profoundly modify the iron-to-oxygen coordination. These differences remain widely undetected by powder X-ray diffraction. EXAFS further confirms that the promotors act as structural modifiers.

This has been studied further by analyzing the EXAFS of chromium in cat 4. In this way the coordination of the impurity can be analyzed rather than the effect of the impurity on the host lattice which has been seen in the Fe EXAFS.

In Fig. 12 the near edge structures of the chromium absorptions are shown for cat 4 in the precursor state and after use. Oxides with chromium in the Cr^{3+} and Cr^{6+} oxidation states were measured as references. It is clear that the oxidation state of chromium changes from 6+ to 3+ during activation of the catalyst. The preedge feature characteristic of a tetrahedral environment of chromium almost completely disappears upon transformation of the chromium in the trivalent state into an octahedral environment. In both catalyst materials the edge features between 0 and 50 eV are different from those of the corresponding binary oxides. This implies that the promotor is not present as a

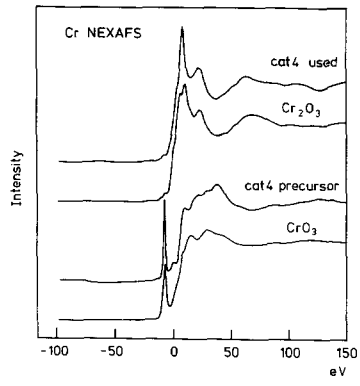

FIG. 12. Chromium K near-edge absorption spectra of cat 4 before and after use in comparison with reference binary chromium oxides. The data were collected in the fluorescence mode.

physical mixture of binary oxide with the iron oxide phase but may be a potassium chromate in the precursor and a iron chromium oxide in the active catalyst.

For further elucidation the EXAFS of the used catalyst was analyzed in detail. Surprisingly it was the transmission data rather than the fluorescence data that gave the best signal-to-noise ratio despite having an adsorption edge jump of only 0.1 corresponding to 0.7 at.% chromium in the sample. Figure 13 shows the quality of the data together with a fit to a model of the first two coordination shells. This model resulted in two maxima of the radial distribution function at 2.00(2) and 3.00(2) Å, with occupations of 5(1) and 7(1), respectively. This model finding 5(1) oxygen in the first shell and 7(1) iron in the second shell is consistent with an octahedral environment of chromium within an iron oxide. A total of six iron–chromium–oxygen structures in the literature were analyzed for reference, yielding Fe–Cr distances of 2.7 to 2.8 Å for direct neighborhood and 3.3 Å for bonding via an oxygen link.

In summary, EXAFS of a promotor atom has illustrated that in the precursor state the promotor is present in an inactive form (Cr^{6+}). This form is thermodynamically unstable under the mildly reducing conditions

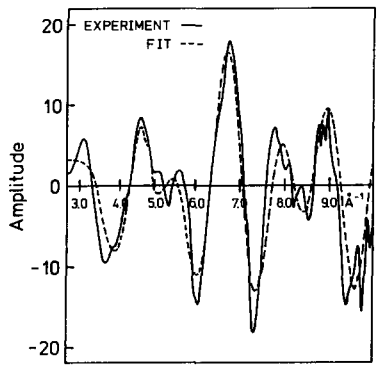

FIG. 13. EXAFS spectrum of chromium in the used cat 4 in comparison to the back Fourier transform of the best fit of the first two coordination shells. The conent of the material in chromium was 0.8 wt%.

of the catalyst operation causing the reduction to Cr^{3+}. In this form the promotor is active and can penetrate the iron oxide lattice to form a ternary oxide. The formation of this compound exerts a cooperative influence on the whole material as can be seen from the Fe EXAFS and the modified chemical reactivity against reduction.

3.6. In Situ X-Ray Diffraction

All results described so far were taken from samples after operation as catalysts and consistently indicate the presence of a spinel iron oxide host lattice with a ternary potassium iron oxide interdispersed, and in addition small amounts of a different potassium iron oxide present as poorly crystalline material. To check the relevance of these components of the catalyst for its functioning it is necessary to study the phase composition *in situ* under reaction conditions. This experiment, in addition, will allow us to decide whether the crystallinity of the constituting phases is different under reaction conditions from the poor quality found in the experiments at room temperature.

The first experiment with catalyst 3 was done to establish the stability of the precursor phases Fe_3O_4 and $K_2Fe_{22}O_{34}$ at 873 K in water vapor. The ternary oxide is perfectly stable under these conditions as can be seen from the relevant sections of the diffraction patterns displayed in Fig. 14. Even prolonged exposure causes little change either in intensity or in lineshape of the reflections from $K_2Fe_{22}O_{34}$. The stability of this phase, which is a suitable candidate for potassium storage material in the working catalyst, is not expected because of the known instability of $K_2Fe_{22}O_{34}$ against liquid water or moisture at room temperature leading to hydrolysis into binary iron oxide and basic potassium carbonate.

The second experiment carried out with activated cat 1 was done to identify the possible existence of a liquid film of potassium hydroxide under reaction conditions. This film can be identified using the inelastic (non-Bragg) scattering from amorphous ma-

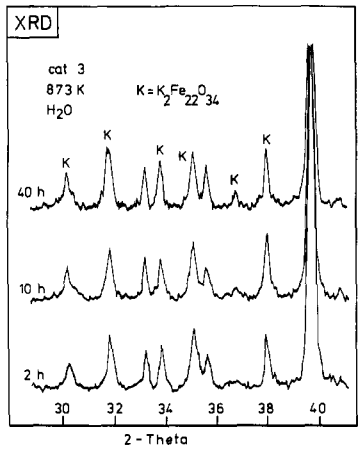

FIG. 14. *In situ* XRD of cat 3 in its fresh state. Conditions were 873 K and 1 atm of steam. The intense peak near 40° 2θ arises from the platinum sample holder.

terial. The relevant experimental data are shown in Fig. 15. The reference was a thin film of KOH deposited from a 0.1 *N* aqueous solution on the platinum sample holder. After drying, the Bragg diffraction patterns of both KOH and basic potassium carbonate were observed. Heating to 873 K resulted in

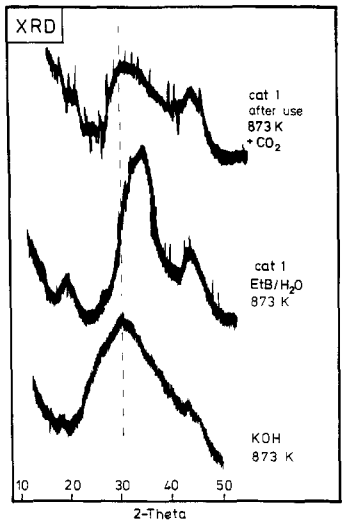

FIG. 15. Inelastic wide-angle scattering profiles of cat 1 and of molten reference KOH as a thin film under reaction conditions. The Bragg peaks are removed. The dashed line serves as a guide to the eye.

the characteristic pattern of a liquid displayed at the bottom of Fig. 15. The Bragg pattern of potassium carbonate which is still stable at 873 K was found to be superimposed as very sharp spikes on the pattern and was omitted for display.

The inelastic scattering patterns from the activated and the *in situ* CO_2-treated catalyst are of significantly different shape and give no evidence for a liquid film of KOH. The inelastic background of the active catalyst does not exhibit any liquidlike structure but indicates the presence of structural disorder in the spinel phase. It is interesting to note that treatment with CO_2 modifies the inelastic scattering from the sample, indicating a bulk structural effect of the catalyst poison.

The third *in situ* experiment was done to identify structural changes in a preactivated catalyst subjected to steam treatment at 873 K. This experiment, modeling the industrial regeneration procedure, was done with catalyst 1 and its results are displayed in Fig. 16. The preactivated catalyst exhibits only the diffraction pattern of the spinel phase (bottom trace in Fig. 16). The (311) reflection (main peak) is broader than all other reflections which exhibit the natural linewidth of the instrument. This increased linewidth of a single reflection points to some anisotropic structural disorder and is another hint to the model of intergrown potassium layers in stacks of spinel blocks.

Steaming modifies the structure in several respects. First the occurrence of a new intense line is observed. This line is the (200) reflection of $KFeO_2$. Further, the pattern of the spinel phase is shifted to slightly lower *d*-values relative to the sample holder Pt reference line, indicating a shrinkage of the lattice parameter. Any quantitative evaluation of the effect which was also observed with catalyst 4 (see Fig. 8) is difficult due to the inadequate geometric stability of the hot stage sample holder. Finally, the crystalline quality of the spinel phase has decreased as can be seen from the loss of intensity in the Bragg reflections, their increase in line-

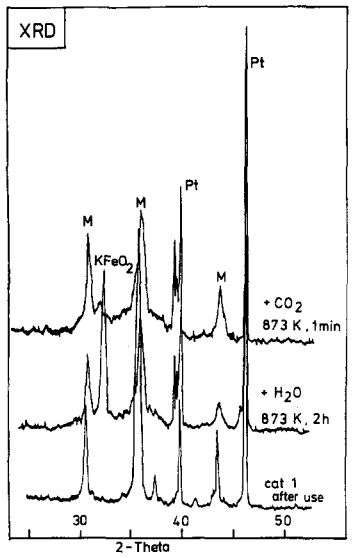

FIG. 16. *In situ* XRD of cat 1. Bottom trace: preactivated at 300 K, central trace: steamed at reaction temperature for 2 h (simulated reactivation), top trace after exposure to CO_2 at 873 K for 1 min. Assignments: M denotes magnetite, and Pt the reference lines of the platinum sample holder.

width, and the pronounced footing of the diffraction peaks.

If the steamed sample is exposed to CO_2 for 1 min the structure changes again. The $KFeO_2$ reflection vanishes almost completely and the structural disorder of the spinel phase further increases. The catalyst poison thus destroys the structure of $KFeO_2$ and deteriorates the crystallinity of the spinel phase. All these results are in basic agreement with the *ex situ* XRD data of Hirano (*12*). In both sets of experiments it was found that the $KFeO_2$ phase is formed from the decomposed to a material that does not yield any Bragg diffraction.

The last *in situ* experiment was designed to proof the relevance of ternary oxide phases in the catalytic reaction. A sample of catalyst 3 was activated *in situ*, and its full accessible diffraction pattern was recorded after 18 h of conversion of etbz to sty. This pattern is displayed in Fig. 17. The intense background at low 2θ arises from X-ray scattering in the steam atmosphere. Under reaction conditions the magnetite matrix coexists with significant amounts of crystalline $K_2Fe_{22}O_{34}$ and $KFeO_2$. The identification of the $KFeO_2$ phase becomes certain because of the occurrence of the only second intense (022) line (at ca. 20° 2θ). The disordered material is associated with the spinel phase, giving rise to the continuous footing between 28° and 48° 2θ.

This state of the catalyst is stable only under reaction conditions. If the material is cooled in nitrogen to room temperature it decomposes within several hours (still under nitrogen) into a mixture of γ-Fe_2O_3, Fe_3O_4, FeOOH, and small amounts of $K_2Fe_{22}O_{34}$. No indication was found for the existence of a crystalline binary potassium compound.

In summary, the *in situ* diffraction experiments provide a very strong indication for identification of the active phase as $KFeO_2$. Under reaction conditions this phase exists as crystalline material with significant abundance. It is metastable at room temperature and under the influence of even traces of moisture. This instability explains the fact that if $KFeO_2$ was identified at all in *ex situ* experiments it occurred as highly disordered material in small quantities.

The time scale of formation and decompo-

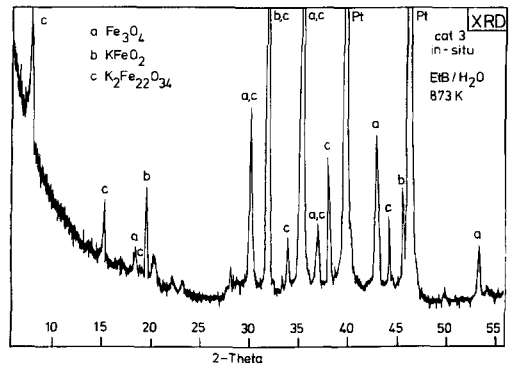

FIG. 17. *In situ* XRD wide scan of cat 3 under synthesis conditions. The atmosphere of steam and ethylbenzene causes the high scattering background below 15° 2θ. The product styrene polymerized at the cold ends of the platinum sample holder.

sition of the X-ray crystalline $KFeO_2$ is of the order of a few hours. Taking into account that the reaction temperature (873 K) is significantly below the synthesis temperature of 1223 K the catalyst material must provide the ingredients potassium oxide and iron oxide in such a way as to ensure high solid-state reactivity, i.e., the materials must be present in a microscopically homogeneous distribution. The matrix structure of $K_2Fe_{22}O_{34}$ in magnetite is a well-suited precursor since it provides reservoirs for both Fe^{3+} ions and potassium ions in a fast ion conducting environment of layers between spinel blocks.

4. DISCUSSION

The bulk structural data obtained for several catalysts with a variety of techniques can now be used to build a general model for the nature of the dehydrogenation catalyst. The catalyst is subject to a permanent restructuring by solid-state reactions. This restructuring occurs not only during initial activation but throughout the whole life of the catalyst as evidenced by the potassium redistribution in two gradients within the grains and within the whole reactor. This solid-state reactivity points to the instability of the active material which is formed and decomposed under reaction conditions. The active material must be a potassium iron oxide (*2, 10, 12*). From the two ternary oxides found, the phase $KFeO_2$ is sensitive to the catalyst poison CO_2 and thus chosen to be the active phase in the model. This choice was confirmed experimentally by showing that independently synthesized $KFeO_2$ exhibits the same catalytic activity as the industrial catalyst. The promotor phases are considered as modifiers influencing the kinetics of the solid-state reactions of the base material potassium iron oxide. They must either be incorporated into the spinel matrix or interact with $KFeO_2$ to stabilize the active phase or to foster its synthesis under reaction conditions.

The relevant facts of the analysis described together with details known from observation of the catalyst performance are accumulated in the schematic life cycle of the catalyst displayed in Fig. 18. This diagram is valid for a prototype catalyst without taking into consideration the optimization effects of promotor additives.

The bulk structure of the precursor materials is quite different for different preparations. With the limited number of catalysts no apparent correlation between phase composition and catalytic performance was found. All precursors contain some hematite, α-Fe_2O_3, and no indication for any known binary potassium compound. Some catalysts contain X-ray crystalline $K_2Fe_{22}O_{34}$. Due to its structure which easily allows for a large nonstoichiometry associated with disorder, it may well be that all precursors contain this phase but only some of them in sufficient crystalline quality to be detectable by power XRD. Details of the calcination process of the precursor may decide over the long-range order of this phase.

If the precursor is subjected to reaction conditions the $K_2Fe_{22}O_{34}$ phase becomes unstable due to the thermodynamically required partial reduction of the iron oxide to magnetite. The presence of water vapor stabilizes the iron oxide against total reduction to iron metal. It is the thermodynamics of the iron oxide–hydrogen–water phase diagram (*24*) that determines the instability of the catalyst precursor at 873 K and that requires that the spinel structure of the matrix accommodate the Fe^{2+} ions. In this structure, nonstoichiometry with respect to an increased amount of Fe^{3+} ions connected with potassium ions can exist in a solid solution. The reduction of Fe^{3+} ions in the lattice forces the K^+ ions to leave the crystal. During this process of partial reduction, which affects all cation positions within the rigid anion lattice, the synthesis of $KFeO_2$ can occur at the edges of the matrix crystals. The lattice mismatch of the structures of the two ternary oxides is so large that internal nucleation would cost too much energy to frequently occur. This active phase at the periphery of the matrix crystal is, however,

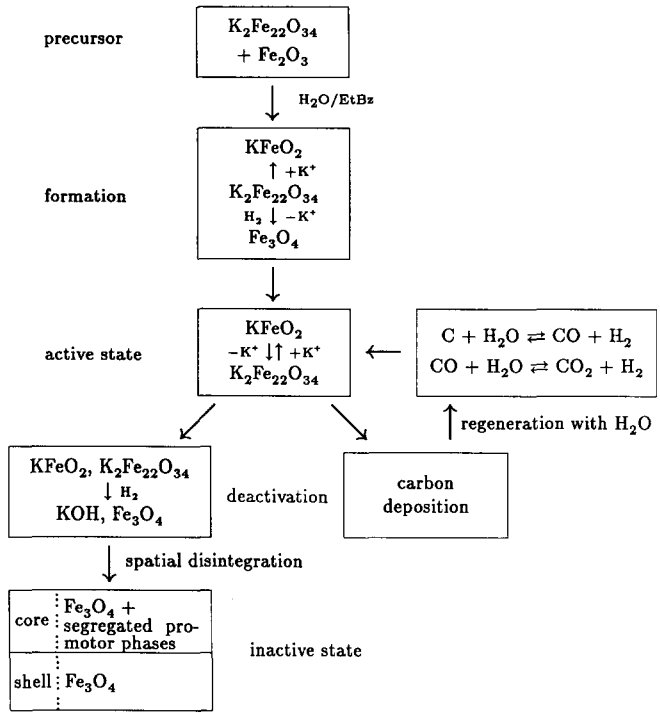

FIG. 18. Schematic life cycle of a prototype catalyst without any promotor additives.

also unstable against partial reduction by the catalytic product hydrogen. The K^+ ions will be liberated again and return by the fast ion conduction mechanism into the matrix crystal exhibiting a lower K^+ concentration at the periphery. This potassium migration through a solid–solid interface below the surface of each catalyst crystal can continue as long as there is an excess of Fe^{3+} ions in the matrix (this excess has been detected by MAS and by the precision lattice constant determination). In essence, the active state is a spinel crystal with excess Fe^{3+} compared to the stoichiometry of Fe_3O_4 (see MAS results). Slow equilibration toward magnetite forces the charge-compensating K^+ ions out of the structure. At the edges of the crystals the phase $KFeO_2$ grows. The catalytic activity of this phase causes its decomposition to magnetite and K^+ ions. As long as there is a gradient for the K^+ ions to migrate back into the storage system of the interspinel block layers the catalyst crystal remains active since renewed reduction of the storage phase causes segregation and renewed growth of the active $KFeO_2$.

This dynamic active state suffers from two principally different modes of deactivation. In industrial practice one discriminates between short-term reversible deactivation and long-term irreversible deactivation. Site blocking by carbon deposition or CO_2 poisoning (not formation of K_2CO_3 which would be stable under reaction conditions) may cause the short-term deactivation. Regeneration with steam results in the potassium-catalyzed gasification of carbon deposits and the structural regeneration of the $KFeO_2$ phase.

The irreversible deactivation is caused by the spatial disintegration of the iron oxide and the potassium compound. At some stage during the life of the catalyst the reducing atmosphere will have allowed the solid to have reached its thermodynamic equilibrium stage, which is highly crystalline stoi-

chiometric magnetite. The irreversible consumption of all excess Fe^{3+} ions is the end of the operation of $K_2Fe_{22}O_{34}$ as storage phase for potassium. It then forms a macroscopic second phase of KOH as it is suggested by the SLP model which this serves as a model for the deactivated catalyst. The volatility of KOH under reaction conditions (the vapor pressure of KOH at 873 K with 0.08 mbar leads to an evaporation rate of ca. 3 nm/s) causes enrichment of KOH within the inner pore system of the catalyst and transport along with the stream of water and organics through the reactor. This potassium redistribution finally causes the inactive state of the catalyst to consist of a potassium-free highly porous shell and a potassium-enriched nonporous core.

The regeneration with steam cannot cure this deactivation for two reasons. First, activation needs to reoxidize some Fe^{2+} to Fe^{3+} to allow the potassium incorporation. Steam alone without traces of air is, however, not an oxidizing agent for magnetite. From thermodynamic properties (*24*) one can estimate the equilibrium constant for the reaction

$$Fe_3O + H_2O \rightarrow \alpha\text{-}Fe_2O_3 + H_2,\ \Delta G = +80.3\ \text{kJ/mole},$$

to be about $K_p = 10^{-5}$. The observed reoxidation of magnetite described by Koppe *et al.* (*13*) is attributed to small amounts of oxygen from air which may have been present in their experiments. Regeneration would thus have to be carried out in an oxidizing atmosphere but not in pure steam.

The second problem with regeneration is the low synthesis temperature for the ternary oxides which was only possible with the fresh precursors due to an intimate distribution of the reactants in suitably disordered matrices achieved in the preparation of the precursors. The spatial disintegration destroyed this intimate mixture and it is expected that regeneration within reasonable times requires at a minimum the temperature of calcination of the precursor (ca. 1200 K) instead of the reactiion temperature of 873 K where regeneration is carried out in practice.

In this picture the most efficient role of the promoters would be to slow down the kinetics of the reduction of the nonstoichiometric spinel iron oxide. This is in full agreement with the experiments that find the stabilization of the matrix against reduction in TG and the incorporation of chromium into the spinel phase.

5. CONCLUSIONS

The bulk analysis of the activated dehydrogenation catalyst led to the conclusion that a ternary potassium iron oxide is the active principle in the catalyst. This oxide is metastable at ambient conditions and was thus not detected in *ex situ* studies. The ternary oxide is also unstable in the reducing atmosphere of the catalytic reaction. It is situated at the edges of crystals which act as storage medium for potassium ions and for excess Fe^{3+} ions. As long as the storage medium is not deactivated by complete reduction of all excess Fe^{3+} to the thermodynamically stable magnetite, this medium provides a matrix for the *in situ* synthesis of the active phase at the surface of the storage crystals. The end of the useful period of the catalyst is reached when all excess Fe^{3+} ions are reduced and the potassium ions start to form a physically separated binary phase of KOH. The high mobility of KOH allows efficient mass transport through the gas phase leading to the potassium gradients observed in analysis of catalysts that have been on stream for several months.

The active catalyst is thus a system that undergoes, under reaction conditions, a series of slow solid-state chemical transformations leading from an initial unstable concentration of defective excess Fe^{3+} ions to the stable situation of stoichiometric well-crystalized magnetite. The lifetime of the catalyst is thus limited by the kinetics of this process which can be affected by promotors and precursor preparation influencing number and organization of the reactive defect centers. This picture further allows us to

rationalize the observed extreme sensitivity of the catalytic performance to minute changes in the reaction conditions, e.g., to the actual ratio between hydrogen and steam at a given temperature.

In this model the catalytic activity is related to a surface containing Fe^{3+} ions and K^+ ions in the ratio 1 : 1. This was already suggested in the model of Lee (*2*). The selectivity may be related to the coverage of the total surface with the active phase; sites with a different chemical composition may be active in conversion of the initial product styrene into undesired materials, a view consistent with the multiple-site hypothesis of Hirano (*6*). The water vapor in the reaction atmosphere is of key importance although it does not take part in the desired reaction of etbz; it moderates the action of the reducing atmosphere onto the iron oxide which would be reduced to the metal without its presence. Considering the high temperature under reaction conditions the mass transport properties are of great importance in allowing short contact times which are necessary to prevent polymerization and gasification of the product styrene. This requirement is closely connected to the morphology of the active catalyst which should, most favorably, be a homogeneous macroporous system.

Parts 2 and 3 of this work will describe the morphological analysis, the identification of the spinel block storage system, and a surface science analysis of the *in situ* activated catalyst.

ACKNOWLEDGMENTS

This work was performed in collaboration with BASF AG Ludwigshafen and supported financially by the Bundesministerium für Forschung und Technologie. The authors acknowledge helpful discussions with Dr. Schwarzmann, Dr. Mross, Dr. Ambach, Dr. Büchele, and others at BASF, and with Professor Wicke and Dr. Bartsch from the University of Münster. The Mössbauer experiments were done in fruitful collaboration with M. Tiedtke and G. Wortmann from the Department of Physics, Free University of Berlin. We thank the SERC for access to the synchrotron facilities at Daresbury Laboratory and for an allocation on the SRS EXAFS service.

REFERENCES

1. Ohlinger, H., and Stadelmann, S., *in* "Ullmann Enzyclopädie der technischen Chemie," Vol. 16, p. 460. Urban Schwarzenberg, Berlin, 1965.
2. Lee, E. H., *Catal. Rev. Sci. Eng.* **8,** 285 (1973).
3. Hirano, T., *Appl. Catal.* **28,** 119 (1986).
4. Carra, S., and Forni, L., *IEC Proc. Des. Dev.* **4,** 281 (1965).
5. Lebedev, N. N., Odabashyan, G. V., Lebedev, V. V., and Markov, M. G., *Kinet. Katal.* **18,** 1177 (1977).
6. Hirano, T., *Appl. Catal.* **26,** 65 (1986).
7. Herzog, D., and Rase, F., *Ind. Eng. Chem. Prod. Res. Dev.* 23, 187 (1984).
8. Mross, W., *in* "Statusseminar: Fortschritte in der Katalyseforschung," BMFT, Bonn p. 173 (1987).
9. Dry, M. E., and Ferreira, L. C., *J. Catal.* **7,** 352 (1967).
10. Vijh, A., *J. Chim. Phys.* **72,** 5 (1975).
11. Bartsch, A., Dissertation thesis, Münster, 1987.
12. Hirano, T., *Appl. Catal.* **26,** 81 (1986).
13. Koppe, J., Rathel, I., and Kraak, P., *Chem. Techn.* **40,** 81 (1988).
14. Scholder, R., and Mansmann, M., *Z. Anorg. Allg. Chem.* **321,** 246 (1963).
15. Sing, K. S. W., and Turk, D. H., *J. Colloid Interface Sci.* **38,** 109 (1972).
16. Barth, T. F. W., *J. Chem. Phys.* **3,** 323 (1935).
17. Pistorius, C. F. W.T., and de Vries, G. F., *Z. Anorg. Allg. Chem.* **395,** 119 (1973).
18. Dudley, G., Steele, B., and Howe, A., *J. Solid State Chem.* **18,** 141 (1976).
19. Howe, A., and Dudley, G., *J. Solid State Chem.* **18,** 149 (1976).
20. Sinha, K. P., and Sihha, A. P. S., *Z. Anorg. Allg. Chem.* **293,** 228 (1958).
21. Sayyed, B. A., Gupta, M. P., Date, S. K., Kamble, K. R., Sonsale, A. Y., and Chatterjee, A. K., *Proc. Indian Acad. Sci.* **95,** 285 (1985).
22. Rethwisch, D. G., and Dumesic, J. A., *Appl. Catal.* **21,** 97 (1986).
23. Greenwood, N. N., and Gibb, R., Mössbauer Spectroscopy," p. 241. Chapman Hall, London, 1971.
24. Barin, I., and Knaake, O., "Thermochemical Properties of Inorganic Substances." Springer, Berlin, 1973.